

# Reactivity of Molecular Dioxygen towards a Series of Isostructural Dichloroiron(III) Complexes with Tripodal Tetraamine Ligands: General Access to $\mu$ -Oxodiiron(III) Complexes and Effect of $\alpha$ -Fluorination on the Reaction Kinetics

Nasser K. Thallaj,<sup>[a]</sup> Olaf Rotthaus,<sup>[a]</sup> Leila Benhamou,<sup>[a, b]</sup> Nicolas Humbert,<sup>[d]</sup> Mourad Elhabiri,<sup>[d]</sup> Mohammed Lachkar,<sup>[b]</sup> Richard Welter,<sup>[c]</sup> Anne-Marie Albrecht-Gary,<sup>[d]</sup> and Dominique Mandon\*<sup>[a]</sup>

**Abstract:** We have synthesized the mono-, di-, and tri- $\alpha$ -fluoro ligands in the tris(2-pyridylmethyl)amine (TPA) series, namely, FTPA, F<sub>2</sub>TPA and F<sub>3</sub>TPA, respectively. Fluorination at the  $\alpha$ -position of these nitrogen-containing tripods shifts the oxidation potential of the ligand by 45–70 mV per added fluorine atom. The crystal structures of the dichloroiron(II) complexes with FTPA and F<sub>2</sub>TPA reveal that the iron center lies in a distorted octahedral geometry comparable to that already found in TPAFeCl<sub>2</sub>. All spectroscopic data indicate that the geometry is retained in solution. These three isostructural complexes all react with molecular dioxygen to yield stable  $\mu$ -oxodiiron(III) complexes. Crystal structure analyses are reported for each of these three  $\mu$ -oxo compounds. With TPA, a symmetrical structure is obtained for a dicationic compound with the tripod coordinated in the  $\kappa^4N$  coordination mode.

With FTPA, the compound is a neutral  $\mu$ -oxodiiron(III) complex with a  $\kappa^3N$  coordination mode of the ligand. Oxygenation of the F<sub>2</sub>TPA complex gave a neutral unsymmetrical compound, the structure of which is reminiscent of that already found with the trifluorinated ligand. On reduction, all  $\mu$ -oxodiiron(III) complexes revert to the starting iron(II) species. The oxygenation reaction parallels the well-known formation of  $\mu$ -oxo derivatives from dioxygen in the chemistry of porphyrins reported almost three decades ago. The striking feature of the series of iron(II) precursors is the effect of the ligand on the kinetics of oxygenation of the complexes. Whereas the parent complex

undergoes 90% conversion over 40 h, the monofluorinated ligand provides a complex that has fully reacted after 30 h, whereas the reaction time for the complex with the difluorinated ligand is only 10 h. Analysis of the spectroscopic data reveals that formation of the  $\mu$ -oxo complexes proceeds in two distinct reversible kinetic steps with  $k_1 \approx 10k_2$ . For TPAFeCl<sub>2</sub> and FTPAFeCl<sub>2</sub> only small variations in the  $k_1$  and  $k_2$  values are observed. By contrast, F<sub>2</sub>TPAFeCl<sub>2</sub> exhibits  $k_1$  and  $k_2$  values that are ten times higher. These differences in kinetics are interpreted in the light of structural and electronic effects, especially the Lewis acidity at the metal center. Our results suggest coordination of dioxygen as an initial step in the process leading to formation of  $\mu$ -oxodiiron(III) compounds, by contrast with an unlikely outer-sphere reduction of dioxygen, which generally occurs at negative potentials.

**Keywords:** iron • kinetics • N ligands • oxo ligands • tripodal ligands

[a] Dr. N. K. Thallaj, Dr. O. Rotthaus, L. Benhamou, Dr. D. Mandon  
Laboratoire de Chimie Biomimétique des Métaux de Transition  
Institut de Chimie, UMR CNRS 7177 - LC 3  
Université Louis Pasteur  
4 rue Blaise Pascal, B.P. 1032, 67070 Strasbourg cedex (France)  
Fax: (+33)390-245-001  
E-mail: mandon@chimie.u-strasbg.fr

[b] L. Benhamou, Prof. Dr. M. Lachkar  
Laboratoire d'Ingénierie des Matériaux Organométalliques  
et Moléculaires  
Université Sidi Mohamed Ben Abdellah, Faculté des Sciences  
BP 1796 (Atlas), 30000 Fez (Morocco)

[c] Prof. Dr. R. Welter  
Laboratoire DECOMET, Institut de Chimie, UMR CNRS 7177  
Université Louis Pasteur  
4 rue Blaise Pascal, B.P. 1032, 67070 Strasbourg cedex (France)

[d] Dr. N. Humbert, Dr. M. Elhabiri, Dr. A.-M. Albrecht-Gary  
Laboratoire de Physico-Chimie Bioinorganique  
Institut de Chimie, UMR CNRS 7177  
Université Louis Pasteur, ECPM  
25, rue Becquerel, 67200 Strasbourg (France)

Supporting information for this article (<sup>1</sup>H NMR spectra for ligands L<sup>1</sup>, L<sup>2</sup> and complexes L<sup>1</sup>FeCl<sub>2</sub>, L<sup>2</sup>FeCl<sub>2</sub>; <sup>1</sup>H NMR monitoring of the oxygenation of complexes L<sup>0</sup>FeCl<sub>2</sub> and L<sup>1</sup>FeCl<sub>2</sub>) is available on the WWW under <http://www.chemeurj.org/> or from the author.

## Introduction

The use of molecular dioxygen ( $O_2$ ) under mild conditions to carry out various oxidation reactions is a particularly important challenge in the current economical context: indeed, most of the processes involved in oxidation chemistry remain expensive and dangerous, and they often involve oxygen donors or/and high temperatures and pressures.<sup>[1]</sup> Considering that chemistry is upstream of many industries, it seems obvious that real effort must be made to meet the goals of “sustainable growth” and “green chemistry”.<sup>[2]</sup>

Interaction of dioxygen with metal-containing biomolecules is a key process in aerobic life; many essential oxidation reactions are carried out by metalloenzymes.<sup>[3–8]</sup>

Historically, the modern biomimetic approach to dioxygen activation by iron complexes started with the chemistry of heme-containing proteins, which led to the development of synthetic porphyrins more than three decades ago.<sup>[9–11]</sup> Non-heme iron-containing enzymes that activate dioxygen are a more recently studied class of metalloproteins in which the metal center at the active site can be either mono- or dinuclear.<sup>[12–14]</sup> With the exception of enzymes for which non innocent substrates such as catechol may modify the electronic structure of the iron center on coordination,<sup>[15,16]</sup> a generally accepted common mechanism involves coordination of dioxygen to a iron(II) center as initial step.<sup>[12]</sup> An alternative and convenient way to generate potentially reactive iron-based species is the so-called shunt reaction involving reaction of metal sites and peroxides, that is, an already reduced form of oxygen, whereas Nature uses molecular dioxygen. This approach has been reviewed, both for proteins and synthetic analogues of active sites, and mechanistic probes have been set up to determine whether high-valent oxo iron species are formed during the catalytic act, or if a radical-based mechanism (Haber–Weiss-like, for instance) is preferred.<sup>[17]</sup>

Only few reports of dioxygen reactivity towards mononuclear non-porphyrinic synthetic iron(II) complexes in the absence of substrates have been made. Very often, the presence of non-innocent ligands such as ( $\alpha$ -ceto) carboxylates, thiolates, or catecholates proved to be crucial.<sup>[18–24]</sup> In some cases, examples of formation of  $\mu$ -oxo dinuclear complexes were reported, and a mechanism that parallels what is described in porphyrin chemistry was discussed.<sup>[20,21,23]</sup> Recently,  $Fe^{II}$  complexes with amide-containing macrocycles were shown to react with dioxygen.<sup>[25]</sup>

A particular case of stabilization of a mononuclear oxoiron(III) product was reported for a complex with a sterically hindered ligand with amido groups.<sup>[26,27]</sup> More recently, a  $\mu$ -oxodiiron complex was also postulated as intermediate in the transfer of an oxygen atom from  $Fe^{IV}$  to  $Fe^{II}$ .<sup>[28]</sup> A few reports describe oxygen-atom transfer reactions from dioxygen to triphenylphosphine, or oxidation of benzylic alcohols to aldehydes by using iron(II) complexes of cyclic amines, or even iron(III) derivatives of tetraamido cyclic ligands, for which a  $\mu$ -oxodiiron(IV) species was characterized.<sup>[29,30]</sup> In these cases, the postulated metal–oxo based mechanism must at least share two common steps: 1) coordination of di-

oxygen to the metal center and 2) formation of potentially reactive intermediates such as peroxidic or high-valent oxoiron species that might react with substrates if present in the medium.

Almost two decades ago, halogenation of porphyrins was shown to induce better activity in oxidation process, as a logical consequence of decreased stability of the oxo intermediates with electron-deficient macrocycles.<sup>[11]</sup> Whereas the biomimetic oxidation chemistry of iron complexes with ligands of the tris(2-pyridylmethyl)amine ( $L^0$  = TPA) type is extremely well documented, only a limited number of reports on halogenated derivatives of this class of ligands is available.<sup>[23,31]</sup> However, it seemed likely that the effect observed with porphyrins would also be found for this ligand class. Following this idea, we already briefly reported several years ago the convenient preparation of tris(2-fluoro-6-pyridylmethyl)amine ( $L^3$  =  $F_3$ TPA), the structure of the corresponding dichloroiron(II) complex, and the fact that dioxygen reacts rapidly with this complex to yield a  $\mu$ -oxodiiron(III) species.<sup>[23]</sup> We then decided to extend the preparation of fluorinated ligands to the mono- and disubstituted tripods ( $L^1$  = FTPA and  $L^2$  =  $F_2$ TPA), and to carry out systematic reactivity studies on the corresponding complexes  $L^nFeCl_2$ , with special attention to oxygen ligation. Here we report a full study of structure and reactivity toward dioxygen of isostructural dichloroiron(II) complexes in the fluorinated TPA series, with the major outcome that dioxygen does coordinate and that Lewis acidity at the metal center is an important parameter with respect to dioxygen ligation. We also report that formation of a  $\mu$ -oxodiiron(III) species is indeed a general reaction if oxygenation is carried out in the absence of a substrate and that, on reduction, the iron(II) starting material can be fully recovered, whereby several oxygenation/reduction cycles are possible.

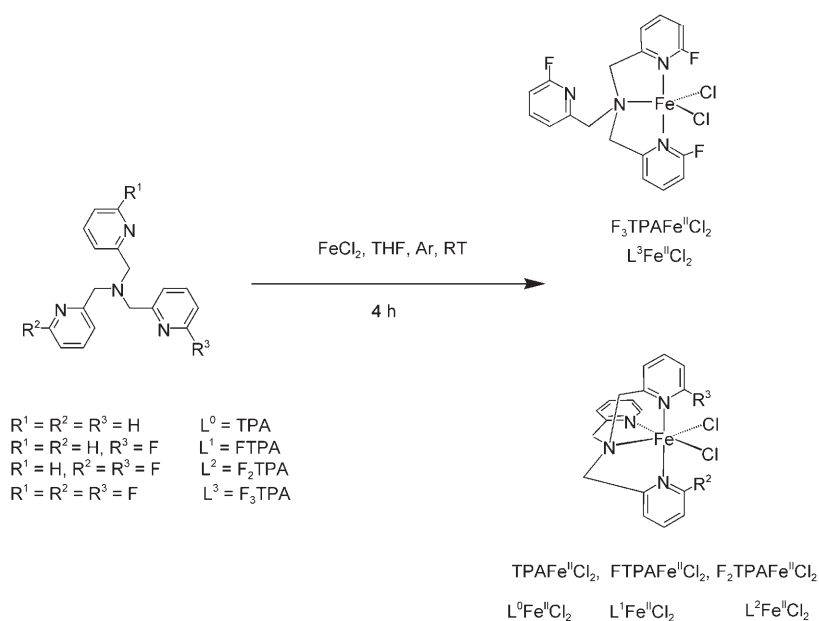
## Results

**Ligand synthesis and electrochemical data:** The key step in the synthesis of the fluorinated ligands is the already reported preparation of 2-fluoro-6-bromomethylpyridine, also used for the synthesis of  $F_3$ TPA.<sup>[23]</sup> Access to the mono-, and difluorinated tripods is easily achieved by reaction of one or two equivalents of this compound with the corresponding secondary and primary amines (bis(2-pyridylmethyl)amine and picolylamine, respectively). Acceptable yields (55 and 59% respectively) could be obtained, and all ligands displayed good stability properties. When electrochemically oxidized, TPA tripods generally undergo irreversible oxidation at the primary amine site.<sup>[32]</sup> To gain insight into the accepting/donating properties of the ligands, we used cyclic voltammetry to measure their anodic potentials (Table 1). Replacement of an  $\alpha$ -hydrogen by a fluorine atom shifts the potential upwards by 45–70 mV; this reflects the expected effect of the halo substituent, and indicates that  $F_3$ TPA is a very electron deficient ligand.

Table 1. Anodic redox potentials of the ligands described in this study. Conditions: CH<sub>3</sub>CN, 0.1 M TBAPF<sub>6</sub> as supporting electrolyte, scan rate 200 mV s<sup>-1</sup>, platinum electrode, SCE reference electrode.

	$E_a$ [mV]	$\Delta E_a(L^n-L^{n-1})$
$L^0$ = TPA	1.118	–
$L^1$ = FTPA	1.166	48
$L^2$ = F <sub>2</sub> TPA	1.236	70
$L^3$ = F <sub>3</sub> TPA	1.281	45

**Preparation of complexes and characterization:** Metalation of the tripods by FeCl<sub>2</sub> was performed by a straightforward method that was already reported for L<sup>0</sup>FeCl<sub>2</sub> and L<sup>3</sup>FeCl<sub>2</sub>.<sup>[23,31]</sup> The compounds are potentially oxygen sensitive, so the reaction must be carried out under inert atmosphere. The reaction is quantitative, the L<sup>n</sup>FeCl<sub>2</sub> complexes are thermally stable, and they are generally yellow. They are soluble in acetonitrile, and were characterized in solution by UV/Vis spectroscopy, paramagnetic <sup>1</sup>H NMR spectroscopy, electrochemical techniques such as molar conductivity and, in certain cases, cyclic voltammetry. The geometry in solution can be deduced from combined analysis of the spectroscopic data. Two kinds of geometry are generally observed for dichloro iron(II) complexes within the class of simple TPA derivatives (Scheme 1).<sup>[31,33]</sup>



Scheme 1. Ligands and dichloroiron(II) complexes discussed in this work. The preparation and structure of F<sub>3</sub>TPAFeCl<sub>2</sub> were already reported.<sup>[23]</sup>

**X-ray diffraction analysis of L<sup>1</sup>FeCl<sub>2</sub> and L<sup>2</sup>FeCl<sub>2</sub>:** Single crystals of both complexes were obtained by layering a solution in acetonitrile with dry, degassed diethyl ether under argon. The ORTEP diagrams (Figure 1 and Figure 2) reveal that the metal center lies in a distorted octahedral environment with the tripod acting as a tetradentate ligand. In

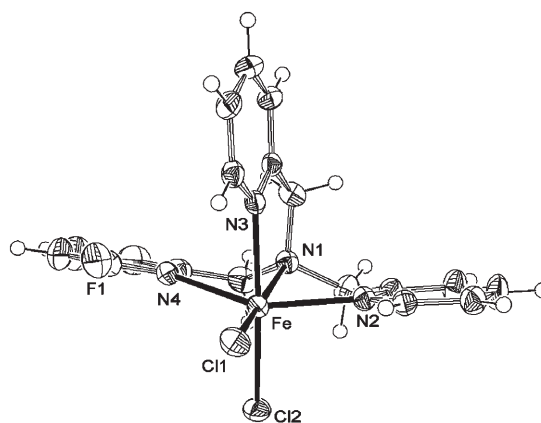


Figure 1. ORTEP diagram of FTPAFeCl<sub>2</sub> with partial numbering scheme. Selected bond lengths [Å] and angles [°]: Fe–N1 2.2937(19), Fe–N4 2.3775(18), Fe–N2 2.2015(17), Fe–N3 2.1766(16), Fe–Cl1 2.3848(9), Fe–Cl2 2.4146(7); N4–Fe–N1 70.67(6), N2–Fe–N1 74.47(7), N3–Fe–N1 77.53(7), Cl2–Fe–Cl1 96.81(3), N4–Fe–Cl2 93.13(5), N2–Fe–Cl2 95.29(6), N3–Fe–Cl1 94.46(5), N1–Fe–Cl2 91.68(5).

L<sup>1</sup>FeCl<sub>2</sub>, the fluoropyridine moiety lies in the equatorial position; in L<sup>2</sup>FeCl<sub>2</sub>, the position of the second fluorine atom is disordered in the ratio 80:20 (equatorial:axial). All distances are longer than 2.1 Å, in line with a high-spin state of the metal center in these complexes. In both complexes, the shortest metal–ligand distances are the axial ones, and that corresponding to the unsubstituted pyridine moiety in L<sup>1</sup>FeCl<sub>2</sub>. The metal to tertiary amine distances are slightly longer. Finally, the longest distances are found between the iron center and the substituted pyridine moieties.

As expected for a five-membered metallacycle, all N–Fe–N angles in both structures involving the tertiary amine lie in the range of 70–78°, that is, distortion with respect to ideal octahedral geometry is severe. As a consequence, the two *trans* pyridine units are not coplanar, and the dihedral angle  $\phi$  can easily be measured. Indeed significant differences are observed on substitution of the parent L<sup>0</sup>FeCl<sub>2</sub> complex, with  $6.7 < \phi < 19.0^\circ$  (Table 2). Also, we noticed that these *trans* pyridine moieties are slightly tilted with respect to each other. For instance, in the structure of L<sup>2</sup>FeCl<sub>2</sub>, one fluorine atom points up, whereas the other is orientated downwards.

We thus defined the torsion angle  $\theta$  involving both *trans* nitrogen atoms and the  $\alpha$ -carbon atom of one of the pyri-

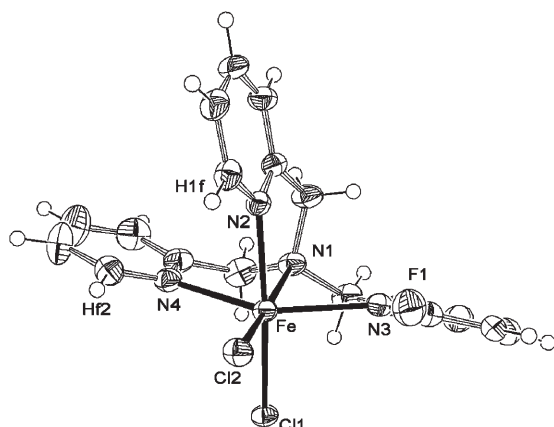


Figure 2. ORTEP diagram of  $F_2TPAFeCl_2$  with partial numbering scheme. The second fluorine atoms are disordered: Hf2 stands for a 80% fluorine-occupied position, and H1f for a 20% fluorine-occupied position. Selected bond lengths [Å] and angles [°]: Fe–N1 2.257(2), Fe–N4 2.342(2), Fe–N3 2.337(2), Fe–N2 2.213(2), Fe–Cl2 2.3361(7), Fe–Cl1 2.4465(7); N4–Fe–N1 74.86(8), N3–Fe–N1 71.58(8), N2–Fe–N1 77.21(7), Cl2–Fe–Cl1 95.97(2), N4–Fe–Cl1 93.09(5), N1–Fe–Cl1 90.83(6), N3–Fe–Cl1 91.73(5), N2–Fe–Cl2 96.30(6).

Table 2. Calculated values of dihedral angle  $\phi$  between the two *trans*-equatorial pyridyl mean planes, torsion angle  $\theta$  between the two *trans*-equatorial pyridyl units and *trans*-angular distortion parameter  $\rho = \phi\theta$  in the pseudo-octahedral complexes (value for  $TPAFeCl_2$  calculated from reference [31]).

	$\phi$ : dihedral angle $Py_t/Py_t$ $\phi$ [°]	$\theta$ : torsion angle $C_a-N_b-N_c-C_d$ $\theta$ [°]	$\rho$ [° <sup>2</sup> ]
$TPAFeCl_2$ ( $L^0FeCl_2$ )	6.75	3.08	20.8
$F_2TPAFeCl_2$ ( $L^1FeCl_2$ )	11.97	2.53	30.3
$F_2TPAFeCl_2$ ( $L^2FeCl_2$ )	19.02	9.26	176.1

dine rings on one side, and the  $\alpha$ -carbon atom of the second *trans* pyridine ring on the other. As a structural parameter to gain insight into the equatorial flexibility of the pyridyl groups around the metal center, we finally introduced the  $\rho$  parameter as the product of  $\phi$  and  $\theta$ . Again, it appears obvious from the values listed in Table 2 that  $\alpha$ -substitution at the pyridyl site induces significant changes in values of  $\rho$ ; the most strongly affected compound is  $L^2FeCl_2$ .

### Solution studies on $L^1FeCl_2$ and $L^2FeCl_2$

**UV/Vis spectroscopy:** Both  $L^1FeCl_2$  and  $L^2FeCl_2$  display ligand-centered transitions at  $\lambda = 258$  nm ( $\epsilon = 11.4 \times 10^3$  mmol<sup>-1</sup>cm<sup>2</sup>) and  $\lambda = 260$  nm ( $\epsilon = 12.2 \times 10^3$  mmol<sup>-1</sup>cm<sup>2</sup>) in acetonitrile. The metal-to ligand charge-transfer (MLCT) transitions appear as well-defined signals at  $\lambda = 415$  nm ( $\epsilon =$

$1.5 \times 10^3$  mmol<sup>-1</sup>cm<sup>2</sup>) and  $\lambda = 390$  nm ( $\epsilon = 1.4 \times 10^3$  mmol<sup>-1</sup>cm<sup>2</sup>) respectively. The values of the molar extinction coefficient suggest that the tripod ligand coordinates in the tetradentate  $\kappa^4N$  mode, as is the case for the parent  $L^0FeCl_2$  complex.<sup>[31]</sup>

**Molar conductivity:** Molar conductivity was measured in the concentration range of 3–5 mM in acetonitrile, and values of  $\Lambda = 31$  S cm<sup>2</sup>mol<sup>-1</sup> and 36 S cm<sup>2</sup>mol<sup>-1</sup> were determined for  $L^1FeCl_2$  and  $L^2FeCl_2$ , respectively. These values lie in the expected range for neutral electrolytes and thus indicate that dissociation must be minor at these concentrations: by comparison,  $\Lambda$  values close to 100 and 150 S cm<sup>2</sup>mol<sup>-1</sup> were found for pure mono- and dicationic species, respectively.<sup>[24,31,34]</sup> All data are listed in Table 3.

**<sup>1</sup>H NMR spectroscopy:** Both spectra exhibit paramagnetically shifted resonances within the range 10–130 ppm, in line with a high-spin state for the metal center in solution. The spectrum of  $L^1FeCl_2$  is qualitatively identical to that already reported for the brominated analogue  $BrTPAFeCl_2$ , and assignment can easily be made by direct comparison.<sup>[31]</sup> The mid-intensity peak width  $\Delta\nu_{1/2}$  decreases in the order  $\alpha-H \geq CH_2 > \beta-H > \gamma-H$ . This is also true of  $L^2FeCl_2$ , which exhibits a simple paramagnetic spectrum. All traces and assignments are given in the Supporting Information.

**Oxygenation of  $L^iFeCl_2$  complexes in solution**

**UV/Vis monitoring:** The color-change observed on saturation of the medium with dry dioxygen could be monitored by UV/Vis spectroscopy. As shown in Figure 3, oxygenation proceeds smoothly for all three complexes. Isosbestic points are pres-

### Oxygenation of $L^iFeCl_2$ complexes in solution

**UV/Vis monitoring:** The color-change observed on saturation of the medium with dry dioxygen could be monitored by UV/Vis spectroscopy. As shown in Figure 3, oxygenation proceeds smoothly for all three complexes. Isosbestic points are pres-

Table 3. Wavelengths, molar extinction coefficients for the MLCT absorptions of  $L^iFeCl_2$  complexes and molar conductivities measured in  $CH_3CN$  at room temperature (value for  $TPAFeCl_2$  obtained from reference [31]).  $F_3TPAFeCl_2$  displays a TBP geometry and exhibits no noticeable absorption in this region.<sup>[23]</sup>

Complex	$\lambda_{MLCT}$ [nm]	$\Delta\lambda_{L^iFeCl_2-L^{i-1}FeCl_2}$	$\epsilon$ [ $10^3$ mmol cm <sup>2</sup> ]	$\Lambda$ [S cm <sup>2</sup> mol <sup>-1</sup> ] ( $3 < c < 5$ mM)
$TPAFeCl_2$ ( $L^0FeCl_2$ )	427.0	–	1.4	30
$F_2TPAFeCl_2$ ( $L^1FeCl_2$ )	415.0	12	1.5	31
$F_2TPAFeCl_2$ ( $L^2FeCl_2$ )	390.0	25	1.4	36
$F_3TPAFeCl_2$ ( $L^3FeCl_2$ )	–	–	–	41

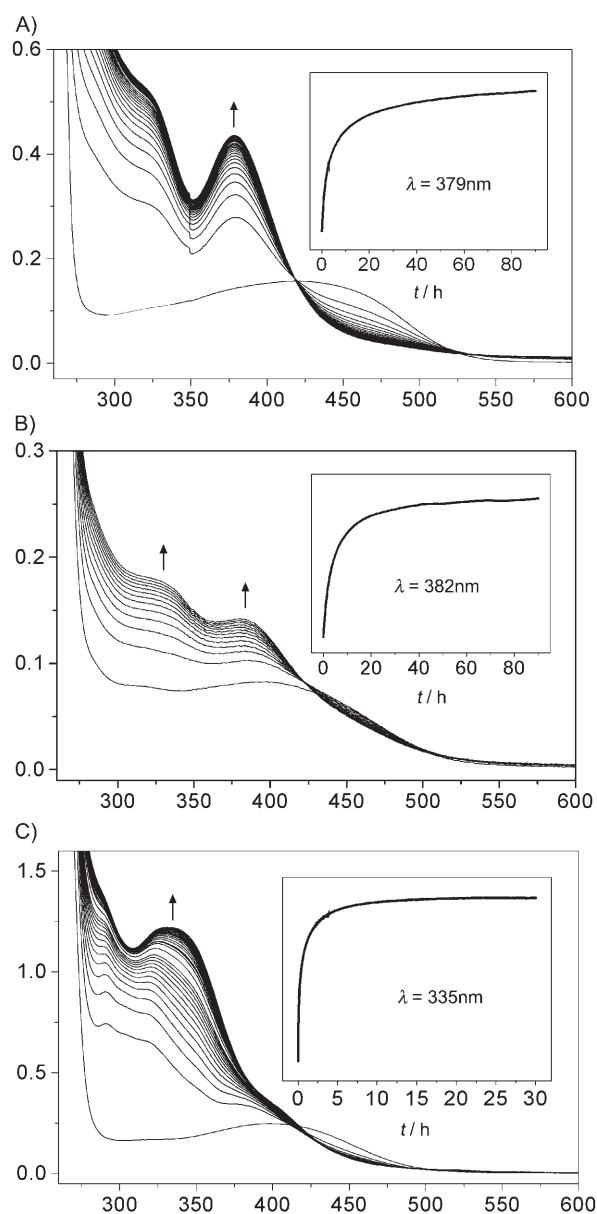


Figure 3. Spectral absorption changes versus time for oxygenation of the pseudo-octahedral dichloroiron(II) complexes  $L^0FeCl_2$  (A),  $L^1FeCl_2$  (B), and  $L^2FeCl_2$  (C) at room temperature in  $CH_3CN$  under  $O_2$ -saturated atmosphere.  $L^0FeCl_2$ : one scan every 120 min,  $L^1FeCl_2$ : one scan every 120 min,  $L^2FeCl_2$ : one scan every 5 min over 1 h, then 1 scan every 15 min. Inset: Variation of absorbance at  $\lambda_{max}$  of the  $\mu$ -oxo complexes versus time.

ent at  $\lambda = 419$  nm for  $L^0FeCl_2$  and 423 nm for  $L^1FeCl_2$ , for which the reaction is considered to be finished after 40 and 30 h, respectively. For these two complexes, the final spectrum exhibits absorptions at  $\lambda = 323.0$  and 379.0 nm ( $\epsilon = 3.1 \times 10^3$  and  $3.5 \times 10^3$   $mmol^{-1}cm^2$ ), and  $\lambda = 328.0$  and 382.0 nm ( $\epsilon = 2.8 \times 10^3$  and  $3.3 \times 10^3$   $mmol^{-1}cm^2$ ), respectively, typical of symmetrical  $\mu$ -oxodiiron(III) compounds.<sup>[35]</sup>  $L^2FeCl_2$  displays a somehow different behavior, since a poorly defined spectrum appears at first, and a stable  $\mu$ -oxo complex characterized by a broad absorption at  $\lambda = 335$  nm ( $\epsilon = 7.0 \times 10^3$   $mmol^{-1}cm^2$ ) for an asymmetric  $\mu$ -oxo derivative is finally

formed.<sup>[36]</sup> In this particular case, the reaction time was shortened to 10 h.

Variation of the spectrophotometric signal at the absorption wavelength of the  $\mu$ -oxo species (Figure 3 insets) with time was analyzed with statistical methods, and clearly evidenced the presence of two well-defined rate-limiting steps. The apparent first-order rate constants  $k_1$  and  $k_2$  were calculated for  $L^0 = TPA$ ,  $L^1 = FTPA$  and  $L^2 = F_2TPA$  and are given in Table 4.

Table 4. First-order rate constants  $k_1$  and  $k_2$  measured for the three iron(II) complexes under  $O_2$ -saturated conditions in  $CH_3CN$ . Uncertainties of  $3\sigma$ , where  $\sigma$  is the standard deviation.

Complex	$k_1$ [ $h^{-1}$ ]	$k_2$ [ $h^{-1}$ ]
$TPAFeCl_2$ ( $TPA = L^0$ )	0.68(6)	0.087(6)
$FTPAFeCl_2$ ( $FTPA = L^1$ )	0.49(6)	0.094(6)
$F_2TPAFeCl_2$ ( $F_2TPA = L^2$ )	7.9(9)	0.61(6)

Regardless of the nature of the organic backbone, the first rate-limiting step proceeds at least five times faster than the second (Table 4). Moreover, it is noteworthy that no spectral amplitude was lost during the mixing procedure, which demonstrates the absence of initial fast steps. Furthermore, no slowest steps were observed and the final absorbance accordingly corresponds to the expected value of the  $\mu$ -oxo complexes with  $L^0$ ,  $L^1$ , and  $L^2$ . A schematic representation of these two rate-limiting steps is displayed in Figure 4.

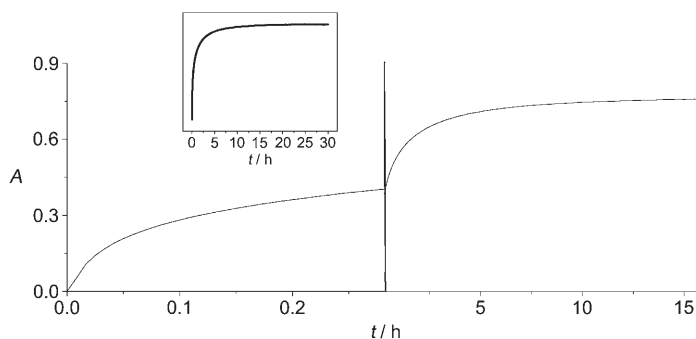


Figure 4. Schematic representation of the two-step kinetics observed during oxygenation of  $L^2FeCl_2$  under  $O_2$ -saturation conditions.

Since  $O_2$  concentrations are similar for each sample, the corresponding kinetic parameters  $k_1$  and  $k_2$  can be compared. As suggested by similar values of  $k_1$  and  $k_2$ ,  $L^0$  and  $L^1$  display similar reactivity towards dioxygen. As indicated above,  $L^2FeCl_2$  stands as an interesting contrast in that its pseudo-first-order rate constants  $k_1$  and  $k_2$  are about one order of magnitude higher.

**$^1H$  NMR monitoring:** Monitoring the oxygenation reaction by  $^1H$  NMR spectroscopy was impossible for  $L^2FeCl_2$  and  $L^3FeCl_3$ , because of precipitation of the reaction products during the reaction. In these cases, only the disappearance

of the starting material could be observed, together with detection of noticeable amounts of free ligand released in the medium. With  $L^0FeCl_2$  and  $L^1FeCl_2$ , however, following the progress of the reaction was possible. With  $L^0FeCl_2$ , the reaction proceeds very smoothly, and the resonances of the new species are concentrated between  $\delta = +40$  and  $-5$  ppm, with a mid-intensity peak width  $\Delta\nu_{1/2}$  between 900 and 150 Hz, in line with the presence of iron(III) species. Ten hours after oxygenation, only a few percent of the starting complex are left. After 24 h, nothing is left of the iron(II) complex.  $L^1FeCl_2$  exhibits similar behavior, with the appearance of new broad ( $300 < \Delta\nu_{1/2} < 2000$  Hz) resonances between 30 and 0 ppm. Over 5 h, about 50% of the starting material is consumed. After 15 h only trace amounts of starting material are detected, and the reaction medium does not change any more with time. All curves are given in the Supporting Information.

Isolation of the oxygenation products revealed that in all cases μ-oxodiiron(III) complexes could be obtained, as displayed in Scheme 2.

### Structure of the oxygenated products isolated as solids

$L^0FeCl_2$ : As mentioned above,  $L^0FeCl_2$  reacts smoothly with dioxygen, and both UV/Vis and  $^1H$  NMR spectroscopy suggest the reaction to be clean.<sup>[37]</sup> The end product could be isolated as a powder by working up the oxygenated acetonitrile solution of the complex (concentration followed by precipitation with diethyl ether and washing several times). Single crystals were obtained by recrystallization from acetonitrile/diethyl ether. Alternatively, layering a freshly oxy-

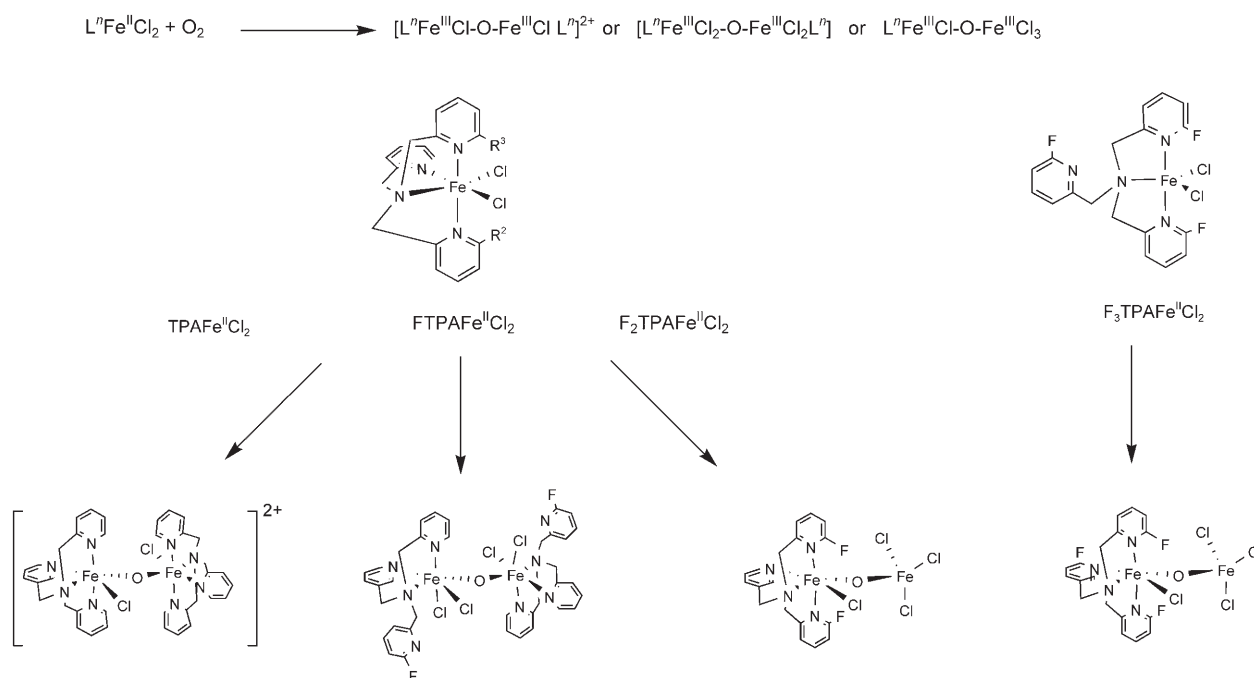
genated solution of the complex with diethyl ether afforded the same crystalline species over two weeks. In parallel to the structural analysis by X-ray diffraction, crystals were dissolved in  $CD_3CN$ , and their spectroscopic data (UV/Vis and  $^1H$  NMR) were shown to be identical to those of the end product detected by direct monitoring of the oxygenation.

The oxygenated compound obtained as a single-crystalline material was the symmetrical μ-oxodiiron(III) species  $[(L^0FeCl)_2O]Cl_2 \cdot 2H_2O$ . The μ-oxo core  $[(L^0FeCl)_2O]^{2+}$  is a dication, and two remote chloride ions are present in the structure, an ORTEP diagram of which is displayed in Figure 5. The ligands coordinate in a *trans* fashion to each other, as shown in the scheme in Table 5.

$L^1FeCl_2$ : The same procedure as described above was applied to  $L^1FeCl_2$ , including spectroscopic characterization of the crystals, which revealed them to share the same data with the end products obtained in solution.

X-ray diffraction analysis revealed that the symmetric μ-oxodiiron(III) compound  $(L^1FeCl_2)_2O \cdot Et_2O$  was obtained (Figure 6). In this compound, the ligands are coordinated *trans* to each other in the “hypodentate” fashion,<sup>[38,39]</sup> that is, only two of the pyridyl units are coordinated to the metal, and the fluorinated ring is a dangling substituent ( $\kappa^3N$  tridentate coordination mode). Each iron atom has pseudo-octahedral geometry, with three nitrogen atoms from the ligand, one oxygen from the μ-oxo bridge and two chloride ligands. As a consequence,  $(L^1FeCl_2)_2O$  is a neutral species.

$L^2FeCl_2$ : Identical procedures to those described above were used. Single crystals were obtained, and their UV/Vis spec-



Scheme 2. Access to μ-oxodiiron(III) compounds by reaction of  $O_2$  with dichloroiron(II) derivatives of the parent TPA and fluorinated ligands. Oxygenation of  $L^3FeCl_2$  has already been reported, and in that case small amounts of a diiron(II) compound were also obtained.<sup>[23]</sup>

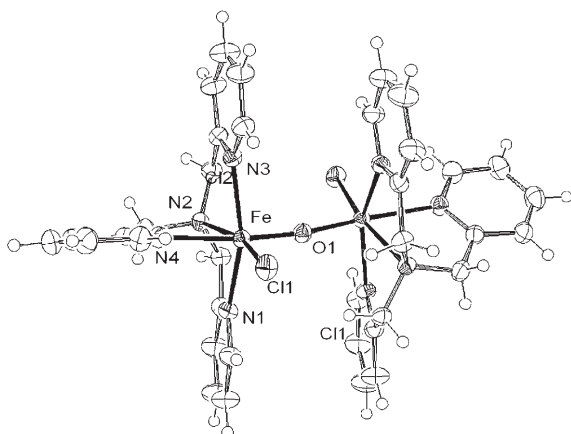


Figure 5. ORTEP diagram of the dication  $[(\text{TPAFeCl})_2\text{O}]^{2+}$  with partial numbering scheme. Selected bond lengths [Å] and angles [°]: Fe–O1 1.7874(4), Fe–Cl1 2.2983(7), Fe–N1 2.165(2), Fe–N4 2.232(2), Fe–N2 2.222(2), Fe–N3 2.139(2), Fe–Fe 3.567(4); N4–Fe–O1 170.40(6), N2–Fe–Cl1 164.62(6), N3–Fe–N1 152.84(9), Fe–O1–Fe 172.22(4).

Table 5. Comparison of structural data for the diiron(III)  $\mu$ -oxo species discussed in this study (data for  $\text{F}_3\text{TPAFe}_2\text{OCl}_4$  obtained from reference [23]).

Ligand	Complex	Fe1–Fe2	Fe1–O	Fe2–O	Fe1–O–Fe2
TPA	 $\kappa^4\text{N}$	3.567	1.788	1.788	172.2
FTPA	 $\kappa^3\text{N}$	3.575	1.793	1.793	170.5
$\text{F}_2\text{TPA}$	 $\kappa^4\text{N}$	3.486	1.771	1.753	163.0
$\text{F}_3\text{TPA}$	 $\kappa^4\text{N}$	3.464	1.757	1.754	161.3

trum was similar to that obtained on oxygenation of the iron(II) precursor.

The compound  $\text{L}^2\text{FeClOFeCl}_3 \cdot \text{CH}_3\text{CN} \cdot \text{Et}_2\text{O}$  was obtained, and its structure is displayed in Figure 7. This structure is very similar to that already reported for the unsymmetrical  $\mu$ -oxo dimer with  $\text{L}^3$  ( $\text{F}_3\text{TPA}$  ligand).<sup>[23]</sup>

Table 5 lists the main structural parameters common to the  $\mu$ -oxodiiron(III) complexes reported in this work.

**Infrared characterization of the  $\mu$ -oxo species:** To detect the asymmetric FeOFe band, solid-state infrared data of  $\mu$ -

oxodiiron(III) complexes were recorded on KBr pellets in the 600–900  $\text{cm}^{-1}$  range and compared to those obtained from the iron(II) precursors. The values of  $\nu_{\text{FeOFe}} = 813$  and  $811 \text{ cm}^{-1}$  for  $[(\text{L}^0\text{FeCl})_2\text{O}]\text{Cl}_2$  and  $[(\text{L}^1\text{FeCl}_2)_2\text{O}]$ , respectively, are comparable to that of  $\nu_{\text{FeOFe}} = 816 \text{ cm}^{-1}$  found for  $[(\text{L}^0\text{FeCl})_2\text{O}](\text{ClO}_4)_2$ , in line with the presence of a symmetrical  $\mu$ -oxo unit.<sup>[35]</sup> In unsymmetrical  $\mu$ -oxodiiron(III) complexes, the asymmetry has been postulated to upshift the  $\nu_{\text{FeOFe}}$  frequency by 30–40  $\text{cm}^{-1}$ .<sup>[36]</sup> Thus, our observation that  $\nu_{\text{FeOFe}} = 873$  and  $868 \text{ cm}^{-1}$  for  $\text{L}^2\text{FeClOFeCl}_3$  and  $\text{L}^3\text{FeClOFeCl}_3$ , respectively, certainly reflects the presence of such asymmetry in our complexes.

**Reduction of the  $\mu$ -oxo complexes:** When a  $\mu$ -oxo complex was stirred in solution in the presence of zinc amalgam under argon, the color gradually turned back to yellow. This could be monitored by UV/Vis spectroscopy, by direct reduction in the cell under anaerobic conditions. The example of the reduction of  $[(\text{L}^0\text{FeCl})_2\text{O}]\text{Cl}_2$  displayed in Figure 8 shows that the reduction is spectroscopically quantitative and yields a spectrum almost identical (but slightly redshifted) to that of the starting material  $\text{L}^0\text{FeCl}_2$ .

For all complexes, the spectra of the iron(II) mononuclear precursors could be detected after 5–10 min of reduction, and we estimated that reduction was quantitative. In the particular case of the reduction of the clean unsymmetrical  $\mu$ -oxo complex  $\text{L}^2\text{FeClOFeCl}_3$ , only half of the intensity of the starting material was obtained, unless the reduction was carried out in the presence of added free ligand, which led to quantitative recovery of the starting signal. Thus, regeneration of a iron(II) complex is possible on reduction of the oxygenated medium, as indicated in Scheme 3.

## Discussion

**General considerations:** The preparation of the ligands is trivial and does not require any particular comment. We paid special attention to the redox potentials of the free ligands, however. As already stated, tripods of the TPA type undergo irreversible oxidation of the aliphatic nitrogen atom at positive potentials.<sup>[32]</sup> In the present work, all compounds were studied under the same experimental conditions to obtain comparable data. Obviously, fluorination increases the oxidation potential of the tripod. Thus, the basicity of the ligands must follow the trend  $\text{TPA} > \text{FTPA} > \text{F}_2\text{TPA} > \text{F}_3\text{TPA}$  with a net effect of 45–70 mV per  $\alpha$ -fluorine atom added to the basic skeleton. It is therefore postulated that for identical structure and geometry in complexes, the Lewis acidity of the metal center M should follow the trend  $\text{F}_3\text{TPA}(\text{M}) > \text{F}_2\text{TPA}(\text{M}) > \text{FTPA}(\text{M}) > \text{TPA}(\text{M})$ .

Metalation of the ligands was achieved by standard methods under dry and strictly anaerobic conditions. We already reported that the geometries of  $\text{L}^0\text{FeCl}_2$  and  $\text{L}^3\text{FeCl}_2$  observed in the solid state are retained in solution.<sup>[23,31]</sup> UV/Vis spectroscopy ( $\epsilon_{\text{MLCT}} > 1.4 \times 10^3 \text{ mmol}^{-1} \text{ cm}^2$ ),  $^1\text{H NMR}$  ( $35 < \Delta\nu_{1/2\beta\text{-}^1\text{H}} < 170 \text{ Hz}$ ) and molar conductivities ( $\Lambda = 31$

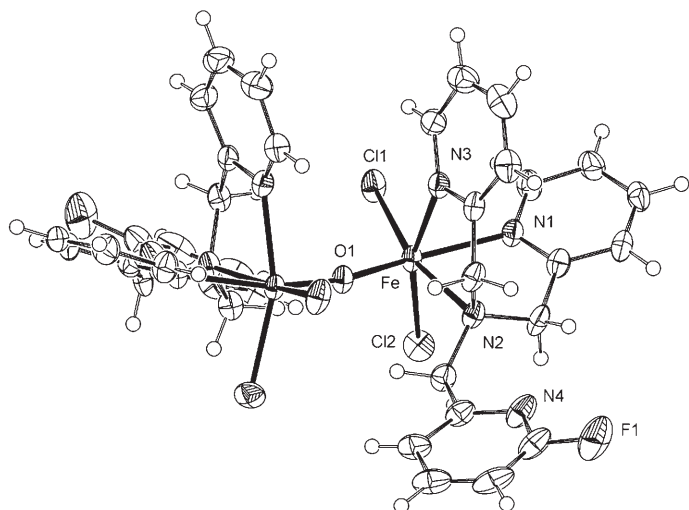


Figure 6. ORTEP diagram of compound  $(\text{FTPAFeCl}_2)_2\text{O}$  with partial numbering scheme. Selected bond lengths [Å] and angles [°]: Fe–O1 1.7934(6), Fe–Cl1 2.3317(12), Fe–N3 2.202(4), Fe–N1 2.274(3), Fe–N2 2.279(3), Fe–Cl2 2.3572(13), Fe–Fe 3.575(4); N1–Fe–O1 163.17(11), N3–Fe–Cl2 160.62(10), N2–Fe–Cl1 164.55(10), Fe–O1–Fe 170.5(3).

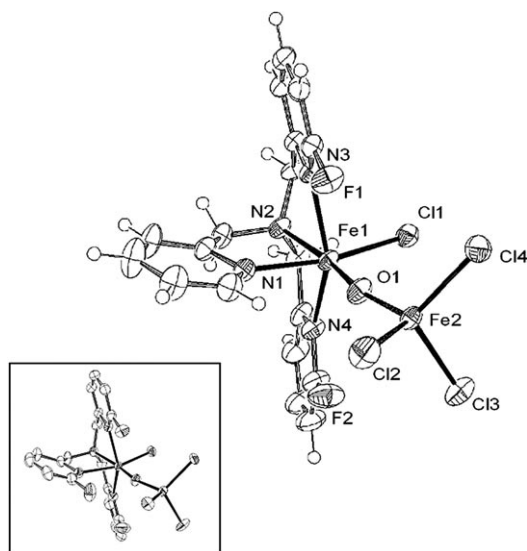


Figure 7. ORTEP diagram of compound  $\text{F}_2\text{TPAFe}_2\text{Cl}_4\text{O}$  with partial numbering scheme. Selected bond lengths [Å] and angles [°]: Fe1–Cl1 2.322(12), Fe1–O1 1.772(3), Fe1–N1 2.143(4), Fe1–N2 2.257(3), Fe1–N3 2.220(3), Fe1–N4 2.196(4), Fe2–O1 1.753(3), Fe2–Cl2 2.2251(13), Fe2–Cl3 2.2320(12), Fe2–Cl4 2.2327(14), Fe1–Fe2 3.486(2); N2–Fe1–N3 74.85(12), N1–Fe1–Cl1 167.03(10), N2–Fe1–O1 171.73(14), Fe1–O1–Fe2 171.73(14). Inset: view of  $\text{F}_3\text{TPAFe}_2\text{Cl}_4\text{O}$ .<sup>[23]</sup>

and  $36 \text{ Scm}^2 \text{ mol}^{-1}$ ) strongly support the same hypothesis for  $\text{L}^1\text{FeCl}_2$  and  $\text{L}^2\text{FeCl}_2$ .

**Structures of the iron(II) complexes:** We previously reported the preparation and structural characterization of the parent  $\text{L}^0\text{FeCl}_2$  and trifluorinated tripod  $\text{L}^3\text{FeCl}_2$  complexes.<sup>[23,31]</sup> Given that fluorine atoms are not particularly bulky groups, these two complexes were expected to be iso-

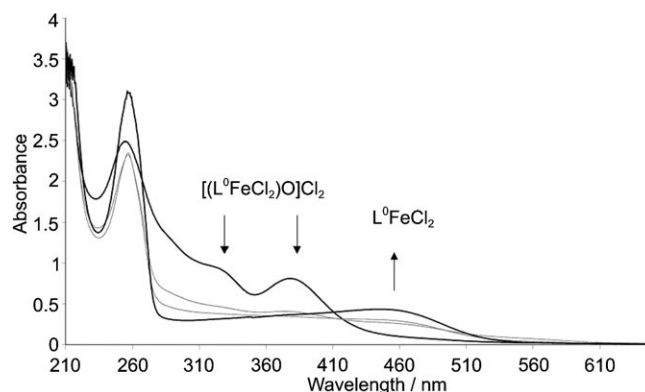
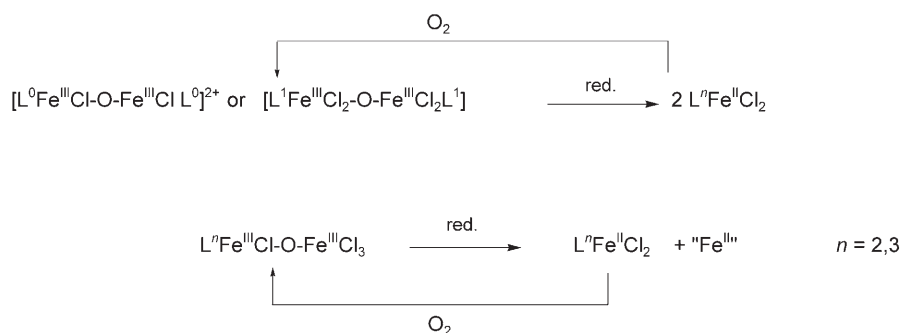


Figure 8. Reduction of  $[(\text{L}^0\text{FeCl}_2\text{O})\text{Cl}_2]$  by zinc amalgam in a UV/Vis cuvette under anaerobic conditions ( $\text{CH}_3\text{CN}$ , RT). Intermediate traces recorded 2 and 4 min after beginning of reduction. Reaction is considered as finished after 6 min.

structural. Thus, direct comparison of the reactivities of these two complexes would have provided insight into the net electronic effect of  $\alpha$  substitution with electronegative groups. In fact, trisubstitution at the  $\alpha$ -position, even with a small atom such as fluorine, proved to be sufficient to induce a trigonal-bipyramidal geometry.<sup>[23]</sup> We thus embarked on the preparation of the mono- $\alpha$ - and di- $\alpha$ -fluorinated ligands, the dichloroiron(II) complexes of which display a distorted  $O_h$  geometry with a  $\kappa^4N$  coordination mode of the ligand. We defined  $\rho$  as a trans-angular distortion parameter in the pseudo-octahedral complexes, resulting from the relative inclination and torsion of the two *trans*-pyridine moieties of the tripod. With  $\rho = 176^\circ$  for  $\text{L}^2\text{FeCl}_2$ , we indeed observed a consequent trans-equatorial distortion. We thus provided an a posteriori explanation why  $O_h$  geometry was not found in  $\text{L}^3\text{FeCl}_2$ : increasing  $\rho$  to a certain point (as result of some repulsion due to trisubstitution) would simply lead to decoordination of one of the equatorial arms of the tripod and give a trigonal bipyramidal geometry.

In the UV/Vis spectrum, the  $O_h$  ( $\kappa^4N$ ) complexes generally display a broad but well-defined MLCT absorption. Halogenation shifts the maximum from  $\lambda = 427 \text{ nm}$  in  $\text{L}^0\text{FeCl}_2$  to  $\lambda = 390 \text{ nm}$  in  $\text{L}^2\text{FeCl}_2$ .

**Structure of the  $\mu$ -oxodiiron(III) compounds:** With  $\text{L}^0$  (TPA), the end oxygenation product is the salt  $[(\text{L}^0\text{FeCl}_2\text{O})\text{Cl}_2]$ . The structure of the cation has already been described twice, once as a perchlorate and once as a mixed-salt counteranion.<sup>[35,40]</sup> In the present work, the presence of two chloride anions does not induce significant changes: the  $\mu$ -oxo moiety exhibits a symmetrical structure in which the tertiary amino groups of both TPA ligands are located *cis* to the  $\mu$ -oxo bridge, and the main structural parameters (metal–metal distances and Fe–O–Fe angles, see Table 5) lie in comparable range to those already reported with the perchlorate counteranion (Fe–Fe 3.565 Å, Fe–O–Fe 175°) and slightly below those observed for the mixed salt (Fe–Fe 3.581 Å, and Fe–O–Fe 180°).<sup>[35,40]</sup>



Scheme 3. From  $\mu$ -oxodiiron(III) to -iron(II) complexes. Conditions: red. = Zn/Hg, CH<sub>3</sub>CN, 5–10 min under argon.

As it is the case for the dichloroiron(II) mononuclear complexes, we now can compare the structural parameters of the complete  $\mu$ -oxo series, that is, from the parent TPA ligand to the  $\alpha$ -trifluorinated tripod (Table 5). A regular and significant decrease in the Fe–O–Fe angle is observed on going from the L<sup>0</sup> (TPA) to L<sup>3</sup> (F<sub>3</sub>TPA) complexes, together with shortening of the Fe–Fe distance. From a qualitative point of view, (L<sup>1</sup>FeCl<sub>2</sub>)<sub>2</sub>O looks like an intermediate situation between the “regular” symmetrical  $\mu$ -oxo derivative found with L<sup>0</sup> and the unsymmetrical complexes with L<sup>2</sup> and L<sup>3</sup>. The ligand here adopts the  $\kappa^3N$  coordination mode. This particular geometry is probably the result of three combined effects: 1) some steric hindrance (which may be weak, since fluoro substituents are not particularly bulky) of the ligand due to  $\alpha$  substitution; 2) possible lower affinity of the electron-deficient pyridine for the metal; and 3) high affinity of chloride ions for the iron(III) center.

#### Recycling $\mu$ -oxodiiron(III) complexes to iron(II) precursors:

In the chemistry of iron(III) complexes with substituted tris(2-pyridylmethyl)amine ligands, we already showed that zinc amalgam is useful to reduce simple iron(III) compounds to the iron(II) state.<sup>[24]</sup> Indeed, in the present study, zinc amalgam was also found to be an easy way to recover the starting material quantitatively for complexes of L<sup>0</sup> and L<sup>1</sup>. When the complexes with L<sup>2</sup> and L<sup>3</sup> were reduced, the spectroscopic yield was not more than 50% for the obvious reason that the diiron(III) compound has only one ligand coordinated (unless additional free ligand was added before reduction). Thus, it is possible to regenerate reactive iron(II) derivatives by reduction of the final  $\mu$ -oxo derivatives.

**Coordination of dioxygen and kinetic studies:** We already reported the fast reaction of L<sup>3</sup>FeCl<sub>2</sub> (in which the metal center exhibits a *tbp* geometry) with O<sub>2</sub> in the absence of substrates, which leads to formation of the unsymmetrical  $\mu$ -oxodiiron(III) complex.<sup>[23]</sup> We now have a series of three complexes L<sup>0–2</sup>FeCl<sub>2</sub> that share the same distorted O<sub>h</sub> geometry, and for which the reaction kinetics vary according to TPAFeCl<sub>2</sub>  $\approx$  FTPAFeCl<sub>2</sub> < F<sub>2</sub>TPAFeCl<sub>2</sub>.

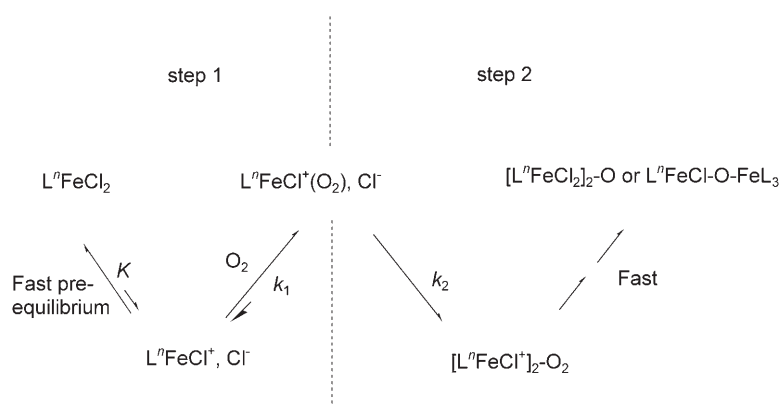
All our complexes display moderately to strongly positive redox Fe<sup>II</sup>/Fe<sup>III</sup> couples.<sup>[41]</sup> The potential of the first reduction of molecular dioxygen is negative with  $E^\circ = -0.73$  V versus SCE in DMSO.<sup>[42,43]</sup> Even if this value is dependent on conditions, it seems very unlikely to reach largely positive values of up to 200 mV or even more that are measured for distorted O<sub>h</sub> complexes.<sup>[41]</sup> We thus believe that a mechanism based on outer-sphere reduction of di-

oxygen is unlikely. By contrast, our kinetic study strongly supports coordination of dioxygen as the initial step of  $\mu$ -oxo formation.

We observed two distinct rate-limiting steps that must reflect coordination of dioxygen to the metal followed by a more complex process leading to formation of the final products (Scheme 4).

Binding of O<sub>2</sub> to the metal center occurs in step 1, which is likely to involve two substeps, that is, decoordination of a ligand from the metal center followed by oxygen ligation. Two ligands could dissociate from the starting iron(II) complexes: 1) one of the pyridyl arms, but this seems very unlikely to occur, since the first spectroscopic step is characterized by an increase in absorbance; 2) more likely, a chloride ion may decoordinate to afford a vacant site for O<sub>2</sub>.<sup>[44]</sup> Since, in the absence of dioxygen in the medium, the molecular conductivity and spectroscopic data indicate that only a very small amount of the complex dissociates in solution, we propose that the first limiting step involves a fast equilibrium leading to L<sup>n</sup>FeCl<sup>+</sup>, followed by slow production of the oxy species.

L<sup>0</sup>FeCl<sub>2</sub> and L<sup>1</sup>FeCl<sub>2</sub> exhibit  $k_1$  and  $k_2$  values that are comparable. Switching to L<sup>2</sup>FeCl<sub>2</sub> affords values of  $k_1$  and  $k_2$  about ten times higher. All three complexes are isostructural. The main structural difference between L<sup>0</sup>FeCl<sub>2</sub> and L<sup>1</sup>FeCl<sub>2</sub> on the one hand and L<sup>2</sup>FeCl<sub>2</sub> on the other is the value of the trans-equatorial distortion parameter  $\rho$ , which switches from 20.8 and 30.3 for the first two complexes to 176.1 for L<sup>2</sup>FeCl<sub>2</sub>. Such a distortion might destabilize the Fe–Cl bond in solution and favor halogenide dissociation (fast pre-equilibrium with stability constant  $K$ , Scheme 4). Considering that the pseudo-first-order rate constant  $k_1$  is associated to binding of O<sub>2</sub> at the vacant site, the increase of  $k_1$  in L<sup>2</sup>FeCl<sub>2</sub> might be due to electronic effects that are significantly different in this particular complex. Obviously, among the three complexes reported here, L<sup>2</sup>FeCl<sub>2</sub> is the one that should display the most pronounced Lewis acidity at the metal center. We also note that the dichloro iron(II) complex of the (6-Me)<sub>3</sub>TPA ligand is insensitive to dioxygen.<sup>[46]</sup> The question of correlating Lewis acidity of the metal center and reactivity of dioxygen has already been addressed in chemical modelling of catechol 1,2-dioxygenases,



Scheme 4. Proposed interpretation of the two kinetic steps involving 1) coordination of  $O_2$  and 2) formation of the  $\mu$ -oxo derivatives.

with the result that high Lewis acidity would confer high oxygenation rates.<sup>[47–50]</sup> We thus postulate that the acceleration observed with  $L^2FeCl_2$  is not only due to structural effects, but also to an increased Lewis acidity at the iron center due to the presence of the two fluoro substituents.

From our kinetic studies, we believe that an oxy form termed  $L^nFeCl(O_2)^+$  must be formed. Trapping this species is a real challenge which we are currently addressing with modified ligands. But further on, what happens in step 2? It seems reasonable to propose that the oxo complex  $L^nFeCl(O_2)^+$  would react with  $L^nFeCl^+$ , again with significant acceleration in the case of the  $L^2FeCl_2$  complex. At the moment, we can only postulate that the reaction would follow a multistep pathway leading to formation of  $\mu$ -oxo complexes, the possibility of which was already mentioned in the chemistry of TPA complexes<sup>[20,23]</sup> or even demonstrated in the chemistry of porphyrins,<sup>[45]</sup>

## Conclusion

The biomimetic relevance of TPA ligands and derivatives no longer remains to be demonstrated. In the chemistry of iron TPA complexes, reaction of dioxygen with a metal center generally requires activation of non-innocent ligands. This is the case for all thiolato-, phenol-, catechol- and benzoyl formate-substituted compounds. Here we reported the preparation of a new series of simple ligands that are easy to obtain and exhibit different electronic properties than those already known in this field. We have fully characterized the corresponding dichloroiron(II) complexes, which react with molecular dioxygen without the need for extra activating ligands, with a noticeable acceleration of the kinetics in the case of the difluorinated ligand. We can now confirm that formation of  $\mu$ -oxodiiron(III) derivatives from iron(II) complexes and dioxygen, as described for porphyrins some thirty years ago, is a general behavior. Coordination of dioxygen is a crucial stage in this multistep process, and our kinetic studies suggest that it is noticeably influenced by the Lewis acidity at the metal center. Transient oxygenated spe-

cies must be generated during oxygenation. The fact that several oxygenation and reduction cycles can be performed should allow conditions for reactivity versus substrates to be set up. Work in this direction is in progress.

## Experimental Section

**General:** Chemicals were purchased from Aldrich Chemicals and used as received. Tris(2-pyridylmethyl)amine (TPA =  $L^0$ ) and bis(2-pyridylmethyl)amine (DPA) were prepared according to published methods.<sup>[51,52]</sup> 2-Fluoro-6-bromomethylpyridine was prepared by a reported procedure.<sup>[23]</sup>  $F_3TPA = L^3$  was prepared by the procedure described in the same reference. All solvents used during the metallation reactions and work-up were distilled and dried according to published procedures<sup>[53]</sup> and degassed shortly before use. Analytical-grade anhydrous  $FeCl_2$  was obtained as a white powder by treating iron powder (ACS grade) with hydrochloric acid in the presence of methanol under an argon atmosphere. Air-sensitive compounds were prepared and handled under argon atmosphere by standard Schlenk techniques.<sup>[23,31]</sup> The purity of the dry dioxygen was 99.99999% (grade 5). Zinc amalgam was prepared by stirring a mixture of 200 g of mercury, 2 g of zinc powder and 100 cm<sup>3</sup> of 25% aqueous sulfuric acid overnight. The acidic phase was removed, and the amalgam thoroughly washed with distilled water until neutral pH, then fresh mercury (5 mL) was added. The resulting amalgam was filtered on a paper skimmer and washed twice with dry THF. It was then left under primary vacuum overnight. Elemental analyses were carried out by the Service d'Analyses de la Fédération de Recherche de Chimie, Université Louis Pasteur, Strasbourg, France.

**Physical methods:** <sup>1</sup>H NMR data were recorded in  $CD_3CN$  for the complexes and  $CDCl_3$  for the ligands at ambient temperature on a Bruker AC 300 spectrometer at 300.1300 MHz with the residual  $CHCl_3$  ( $CD_2HClN$ ) as reference for calibration. The UV/Vis spectra were recorded on a Varian Cary 05 E UV-VIS NIR spectrophotometer equipped with an Oxford instrument DN1704 cryostat in optically transparent Schlenk cells. The kinetic data were analyzed with the commercial software Biokine.<sup>[54]</sup> This program fits up to three exponential functions to the experimental curves with the Simplex algorithm after initialization with a Padé–Laplace method.<sup>[55,56]</sup> Conductivity measurements were carried out under argon at 20 °C with a CDM 210 Radiometer Copenhagen Conductivity Meter and a Tacussel CDC745-9 electrode. Cyclic voltammetric data were obtained with a PAR 173 A potentiostat in a 0.1 M acetonitrile solution of TBAPF<sub>6</sub> (supporting electrolyte) by using platinum and saturated calomel electrodes as reference. For each measurement, the potential was checked by addition of a small amount of ferrocene ( $Fe/Fe^+$ : 0.380 V vs. SCE) to the cell. Infrared spectra were measured in the solid state as KBr pellets on a Perkin-Elmer FT-IR, BX series spectrophotometer.

**Synthesis of  $L^1 = FTPA$ :** 2-Fluoro-6-bromomethylpyridine (1.5 g, 7.89 mmol) was added to a solution of DPA (1.57 g, 7.89 mmol) in ethanol (100 cm<sup>3</sup>).  $Na_2CO_3$  (1.6 g, 15.77 mmol) was added to the mixture. The reaction mixture was heated to 95 °C and stirred for 15 h. The mixture was then cooled to room temperature, and the solvent removed under vacuum. Then water was added and the product was extracted with  $CH_2Cl_2$  (3 × 50 mL). The organic phase was dried over  $MgSO_4$ , and the solvent was removed by rotary evaporation. The residue was extracted with pentane. Concentration of this solution afforded white-orange microcrystals (yield: 1.34 g, 55%). <sup>1</sup>H NMR (300 MHz,  $CDCl_3$ ):  $\delta$  = 3.83 (s, 2H), 3.89 (s, 4H), 6.75 (m, 1H), 7.13 (m, 2H), 7.45 (m, 1H), 7.56 (m,

2H); 7.63 (m, 2H), 7.74 (m, 1H), 8.53 ppm (m, 2H,  $\alpha$ -pyridyl); elemental analysis calcd (%) for  $C_{18}H_{17}N_4F$ : C 70.11, H 5.56, N 18.17, F 6.16; found: C 69.79, H 5.64, N 18.08.

**Synthesis of  $L^2 = F_2TPA$ :** 2-Fluoro-6-bromomethyl pyridine (3 g, 15.78 mmol) was added to a solution of picolylamine (852 mg, 7.89 mmol) in ethanol (150 cm<sup>3</sup>).  $Na_2CO_3$  (3 g, 28.30 mmol) was added to the mixture. The reaction mixture was heated to 95 °C and stirred for 15 h. The mixture was then cooled to room temperature, and the solvent removed under vacuum. Then water was added and the product was extracted with  $CH_2Cl_2$  (3 × 50 mL). The organic phase was dried over  $MgSO_4$ , and the solvent removed by rotary evaporation. The residue was extracted with pentane. Concentration of this solution afforded hygroscopic white-yellow microcrystals. (Yield: 1.51 g, 59%). <sup>1</sup>H NMR (300 MHz,  $CDCl_3$ ):  $\delta$  = 3.86 (s, 4H), 3.94 (s, 2H), 6.77 (m, 2H), 7.19 (m, 1H), 7.48 (m, 2H), 7.63 (m, 1H), 7.67 (m, 1H), 7.70 (m, 2H), 8.55 ppm (m, 1H,  $\alpha$ -pyridyl); elemental analysis calcd (%) for  $C_{18}H_{16}N_4F_2$ : C 66.25, H 4.94, N 17.17; found: C 65.87, H 5.05, N 16.63.

**Oxygenation of iron(II) compounds:** The procedure for  $F_3TPAFeCl_2$  has already been described.<sup>[23]</sup> For  $TPAFeCl_2$ ,  $FTPAFeCl_2$ , and  $F_2TPAFeCl_2$ , we proceeded as follows: iron(II) complex (140 mg) was dissolved in  $CH_3CN$  (50 mL) under argon in a Schlenk tube. Dry dioxygen was bubbled for 15 s, and the medium was kept under oxygen in the closed Schlenk tube and stirred for 48 h. The solvent was then evaporated. The dark solid was washed with diethyl ether. Part of it was dissolved in  $CD_3CN$  for NMR analysis. The rest was dissolved in regular acetonitrile (technical grade), the solution was introduced in glass tubes, and layered with diethyl ether (technical grade). Single crystals formed over several days.

**X-ray analysis:** Single crystals of  $FTPAFeCl_2$ ,  $F_2TPAFeCl_2 \cdot CH_3CN$ ,  $(TPAFeCl_2)_2OCl_2 \cdot (H_2O)_2$ ,  $(FTPAFeCl_2)_2O \cdot Et_2O$  and  $F_2TPAFeCl_2O \cdot CH_3CN \cdot Et_2O$  were mounted on a Nonius Kappa CCD area detector diffractometer ( $\lambda(MoK\alpha) = 0.71073 \text{ \AA}$ ). Quantitative data were obtained at 173 K for all complexes. The complete conditions of data collection (Denzo software) and structure refinements are given in the Supporting Information. The cell parameters were determined from reflections taken from one set of ten frames (1.0° steps in phi angle), each at 20 s exposure. The structures were solved by direct methods (SIR97) and refined against  $F^2$  by using the SHELXL97 software (Kappa CCD Operation Manual, Nonius B.V., Delft, The Netherlands, 1997; G. M. Sheldrick, SHELXL97, Program for the refinement of crystal structures, University of Göttingen, Germany, 1997). Absorption was not corrected. All non-hydrogen atoms were refined anisotropically. Hydrogen atoms were generated according to stereochemistry and refined using a riding model in SHELXL97.

Crystal data for  $FTPAFeCl_2$ : Yellow crystals, monoclinic, space group  $P2_1/n$ ,  $a = 9.3920(10)$ ,  $b = 13.784(2)$ ,  $c = 14.617(2) \text{ \AA}$ ,  $\beta = 103.31(5)^\circ$ ,  $V = 1841.5(4) \text{ \AA}^3$ ,  $\rho_{calcd} = 1.569 \text{ g cm}^{-3}$ ,  $Z = 4$ . For 5381 unique, observed reflections with  $I > 2\sigma(I)$  and 235 parameters, the discrepancy indices were  $R = 0.041$  and  $R_w = 0.096$ .

Crystal data for  $F_2TPAFeCl_2 \cdot CH_3CN$ : Yellow crystals, monoclinic, space group  $P2_1/c$ ,  $a = 10.0780(6)$ ,  $b = 14.0300(9)$ ,  $c = 15.4080(10) \text{ \AA}$ ,  $\beta = 97.500(3)$ ,  $V = 2160.0(2) \text{ \AA}^3$ ,  $D_{calcd} = 1.520 \text{ g cm}^{-3}$ ,  $Z = 4$ . For 6313 unique, observed reflections with  $I > 2\sigma(I)$  and 270 parameters, the discrepancy indices were  $R = 0.054$  and  $R_w = 0.100$ .

Crystal data for  $(TPAFeCl_2)_2OCl_2 \cdot (H_2O)_2$ : Dark red crystals, monoclinic, space group  $C2/c$ ,  $a = 15.740(3)$ ,  $b = 16.460(3)$ ,  $c = 16.050(3) \text{ \AA}$ ,  $\beta = 111^\circ$ ,  $V = 3881(2) \text{ \AA}^3$ ,  $\rho_{calcd} = 1.520 \text{ g cm}^{-3}$ ,  $Z = 4$ . For 3492 unique, observed reflections with  $I > 2\sigma(I)$  and 240 parameters, the discrepancy indices were  $R = 0.038$  and  $R_w = 0.064$ .

Crystal data for  $(FTPAFeCl_2)_2O \cdot Et_2O$ : red crystals, tetragonal, space group  $I41cd$ ,  $a = b = 17.4410(5)$ ,  $c = 27.0270(7) \text{ \AA}$ ,  $V = 8221.3(4) \text{ \AA}^3$ ,  $\rho_{calcd} = 1.505 \text{ g cm}^{-3}$ ,  $Z = 8$ . For 4836 unique, observed reflections with  $I > 2\sigma(I)$  and 263 parameters, the discrepancy indices were  $R = 0.042$  and  $R_w = 0.108$ .

Crystal data for  $F_2TPAFeCl_2O \cdot CH_3CN \cdot Et_2O$ : Yellow crystals, triclinic, space group  $P-1$ ,  $a = 10.4000(10)$ ,  $b = 14.4760(10)$ ,  $c = 16.177(2) \text{ \AA}$ ,  $\alpha = 82.244(5)$ ,  $\beta = 71.479(5)$ ,  $\gamma = 64.457(5)^\circ$ ,  $V = 1507.9(3) \text{ \AA}^3$ ,  $\rho_{calcd} =$

$1.428 \text{ g cm}^{-3}$ ,  $Z = 2$ . For 8811 unique, observed reflections with  $I > 2\sigma(I)$  and 306 parameters, the discrepancy indices are  $R = 0.063$  and  $R_w = 0.189$ . CCDC 653837, 653838, 653839, 653840 and 653841 contain the supplementary crystallographic data for this paper. These data can be obtained free of charge from The Cambridge Crystallographic Data Centre via [www.ccdc.cam.ac.uk/data\\_request/cif](http://www.ccdc.cam.ac.uk/data_request/cif).

## Acknowledgements

This work was supported as a collaborative action between CNRS (project n° 18552 - France) and CNRST (project n° chimie 08/06 - Morocco). Both organizations are gratefully acknowledged for their support. We also thank Dr Remy Louis, head of the Institut de Chimie in Strasbourg, for constant support and encouragement, and the ULP. The Conseil Scientifique de l'ULP is acknowledged for specific support (n° AO CS ULP 2006).

- [1] J. A. Labinger, *J. Mol. Catal. A* **2004**, *220*, 27–35.
- [2] P. T. Anastas, J. C. Warner, *Green Chemistry: Theory and Practice*, Oxford University Press, New York, **1998**.
- [3] J. J. R. Frausto da Silva, R. J. P. Williams, *The Biological Chemistry of the Elements—The Inorganic Chemistry of Life*, Clarendon Press, Oxford, **1991**.
- [4] W. Kaim, B. Schwedereski, *Bioinorganic Chemistry: Inorganic Elements in the Chemistry of Life. An Introduction and Guide*, Wiley, Chichester, **1994**.
- [5] S. J. Lippard, J. M. Berg, *Principles of Bioinorganic Chemistry*, University Science Books, Mill Valley, **1994**.
- [6] R. Roat-Malone, *Bioinorganic Chemistry—A Short Course*, Wiley-Interscience, Hoboken, New Jersey, **2002**.
- [7] P. C. Cirino, F. H. Arnold, *Curr. Opin. Chem. Biol.* **2002**, *6*, 130–135.
- [8] *Bioinorganic Catalysis*, 2nd ed. (Ed.: J. Reedijk), Marcel Dekker, New York, **1999**.
- [9] T. L. Poulos in *Heme Proteins, Vol. 7* (Eds.: G. L. Eichhorn, L. G. Marzilli), Elsevier, Amsterdam, **1988**.
- [10] J. P. Collman, R. G. Gagne, C. A. Reed, T. H. Halbert, G. Lang, W. T. Robinson, *J. Am. Chem. Soc.* **1975**, *97*, 1427–1439.
- [11] *The Porphyrin Handbook*, (Eds.: K. M. Kadish, K. M. Smith, R. Guilard), Academic Press, San Diego, **2000**.
- [12] E. I. Solomon, T. C. Brunold, M. I. Davis, J. N. Kemsley, S.-K. Lee, N. Lehnert, F. Neese, A. J. Skulan, Y. S. Yang, J. Zhou, *Chem. Rev.* **2000**, *100*, 235–349.
- [13] M. Costas, M. P. Mehn, M. P. Jensen, L. Que, Jr., *Chem. Rev.* **2004**, *104*, 939–986.
- [14] J. Du Bois, T. J. Mizoguchi, S. J. Lippard, *Coord. Chem. Rev.* **2000**, *200–202*, 443–485.
- [15] M. W. Wething, L. P. Wackett, L. Que, Jr., J. D. Lipscomb, D. H. Ohlendorf, *J. Bacteriol.* **2004**, *186*, 1945–1958.
- [16] D.-H. Jo, L. Que, Jr., *Angew. Chem.* **2000**, *112*, 4454–4457; *Angew. Chem. Int. Ed.* **2000**, *39*, 4284–4287.
- [17] M. Costas, K. Chen, L. Que, Jr., *Coord. Chem. Rev.* **2000**, *200–202*, 517–544.
- [18] Y. C. Min, L. Que, Jr., *J. Am. Chem. Soc.* **1995**, *117*, 3999–4013.
- [19] N. Kitajima, N. Tamura, H. Amagai, H. Fukui, Y. Moro-oka, Y. Mizutani, T. Kitagawa, R. Mathur, K. Heerwegh, C. A. Reed, C. R. Randall, L. Que, Jr., K. Tatsumi, *J. Am. Chem. Soc.* **1994**, *116*, 9071–9085.
- [20] Y. Zang, L. Que, Jr., *Inorg. Chem.* **1995**, *34*, 1030–1035.
- [21] R. M. Theisen, J. Shearer, W. Kaminsky, J. A. Kocacs, *Inorg. Chem.* **2004**, *43*, 7682–7690.
- [22] D.-H. Jo, Y. M. Chiou, L. Que, Jr., *Inorg. Chem.* **2001**, *40*, 3181–3190.
- [23] A. Machkour, D. Mandon, M. Lachkar, R. Welter, *Inorg. Chem.* **2004**, *43*, 1545–1550.

- [24] A. Machkour, N. K. Thallaj, L. Benhamou, M. Lachkar, D. Mandon, *Chem. Eur. J.* **2006**, *12*, 6660–6668.
- [25] I. V. Korendovytych, O. P. Kryatova, W. M. Reiff, E. V. Rybak-Akimova, *Inorg. Chem.* **2007**, *46*, 4197–4211.
- [26] C. E. MacBeth, A. P. Golombek, V. G. Young Jr., C. Yang, K. Kuczera, M. P. Hendrich, A. S. Borovik, *Science* **2000**, *289*, 938–941.
- [27] C. E. MacBeth, R. Gupta, K. Mitchell-Koch, V. G. Young, Jr., G. H. Lushington, W. H. Thompson, M. P. Hendrich, A. S. Borovik, *J. Am. Chem. Soc.* **2004**, *126*, 2556–2567.
- [28] C. V. Sastri, K. Oh, Y. J. Lee, M. S. Seo, W. Shin, W. Nam, *Angew. Chem.* **2006**, *118*, 4096–4099; *Angew. Chem. Int. Ed.* **2006**, *45*, 3992–3995.
- [29] S. O. Kim, C. V. Sastri, M. S. Seo, J. Kim, W. Nam, *J. Am. Chem. Soc.* **2005**, *127*, 4178–4179.
- [30] A. Gosh, F. Tiago de Oliveira, T. Yano, T. Nishioka, E. S. Beach, I. Kinoshita, E. Münck, A. D. Ryabov, C. P. Horwitz, T. J. Collins, *J. Am. Chem. Soc.* **2005**, *127*, 2505–2513.
- [31] D. Mandon, A. Machkour, S. Goetz, R. Welter, *Inorg. Chem.* **2002**, *41*, 5363–5372.
- [32] A. G. Blackman, *Polyhedron* **2005**, *24*, 1–39.
- [33] A particular case of square-pyramidal geometry has been observed in the solid state as a result of stacking effects with a tripod substituted by a potentially coordinating ligand: N. K. Thallaj, A. Machkour, D. Mandon, R. Welter, *New J. Chem.* **2005**, *29*, 1555–1558.
- [34] T. J. Hubin, J. M. McCormick, S. R. Collinson, M. Buchalova, C. M. Perkins, N. W. Alcock, P. K. Kahol, A. Raghunatan, D. H. Busch, *J. Am. Chem. Soc.* **2000**, *122*, 2512–2522.
- [35] A. Hazell, K. B. Jensen, C. J. McKenzie, H. Toftlund, *Inorg. Chem.* **1994**, *33*, 3127–3134.
- [36] P. Gomez-Romero, E. H. Witten, W. M. Reiff, G. Backes, J. Sanders-Loehr, G. B. Jameson, *J. Am. Chem. Soc.* **1989**, *111*, 9039–9047.
- [37] The amount of free TPA ligand released once oxygenation is over is estimated to be less than 5% on the basis of integration of the ligand signals in the  $^1\text{H}$  NMR tube that was used for NMR monitoring of the reaction with  $\text{O}_2$  (see Supporting Information).
- [38] A. G. Blackman, *C. R. Chim.* **2004**, *8*, 107–119.
- [39] E. C. Constable, *Prog. Inorg. Chem.* **1994**, *42*, 67–138.
- [40] T. Kojima, R. A. Leising, S. Yan, L. Que, Jr., *J. Am. Chem. Soc.* **1993**, *115*, 11328–11335.
- [41] The electrochemical behavior of our compounds with substituted tripods seems to be complex and will be the subject of a forthcoming article. Cyclic voltammetry on  $\text{L}^0\text{FeCl}_2$  affords a nicely reversible and well-defined wave at  $E_{1/2} = 195$  mV versus SCE.  $\text{L}^{-3}\text{FeCl}_2$  complexes display a different behavior, which suggests that, unlike under neutral conditions (e.g., in  $\text{CH}_3\text{CN}$ , in which the structures are retained in solution), the use of a strongly dissociating medium (e.g., a 0.1 M solution of supporting electrolyte) leads to dissociation and aggregation of the complexes, since multiple waves are detected at positive potential.
- [42] A. D. Goolsby, D. T. Sawyer, *Anal. Chem.* **1968**, *40*, 83–86.
- [43] J. S. Valentine, A. E. Quinn, *Inorg. Chem.* **1976**, *15*, 1997–1999.
- [44] This hypothesis is supported by the following experimental facts: working in non-dissociating solvents such as  $\text{CH}_2\text{Cl}_2$  decreases the reaction rate by a factor of ten; also, “freezing” the chloride ions at the metal site by hydrogen bonding with an  $\alpha$ -amido-substituted ligand impedes the oxygenation reaction: L. Benhamou, H. Jaafar, A. Wane, D. Mandon, unpublished results.
- [45] D. H. Chin, J. Del Gaudio, G. La Mar, A. Balch, *J. Am. Chem. Soc.* **1977**, *99*, 5486–5488.
- [46] OL. Benhamou, D. Mandon, unpublished results
- [47] M. Velusamy, R. Mayilmurugan, M. Palaniandavar, *Inorg. Chem.* **2004**, *43*, 6284–6293.
- [48] D. D. Cox, L. Que Jr, *J. Am. Chem. Soc.* **1988**, *110*, 8085.
- [49] D. D. Cox, S. J. Benkovic, L. M. Bloom, F. C. Bradeley, M. J. Nelson, L. Que, Jr., D. E. Wallick, *J. Am. Chem. Soc.* **1988**, *110*, 2026.
- [50] H. G. Jang, D. D. Cox, L. Que, Jr., *J. Am. Chem. Soc.* **1991**, *113*, 9200.
- [51] M. S. Nelson, J. Rodgers, *J. Chem. Soc. A* **1968**, 272–276
- [52] G. Anderegg, F. Wenk, *Helv. Chim. Acta* **1967**, *50*, 2330–2332.
- [53] W. L. F. Armarego, D. D. Perrin, *Purification of Laboratory Chemicals*, 4th ed., Pergamon Press, Oxford, **1997**.
- [54] Biokine V3.0 User’s Manual, Bio-Logic Company, Echirolles, France, **1991**.
- [55] J. A. Nelder, R. Mead, *Comput. J.* **1965**, *7*, 308–313.
- [56] E. Yeramian, P. Claverie, *Nature* **1987**, *326*, 169–174.

Received: December 12, 2007

Revised: April 1, 2008

Published online: June 18, 2008